Interferometric device for the in-process measurement of diameter variation in the manufacture of ultraprecise spheres

OPEN ACCESS
IOP Publishing
Measurement Science and Technology
Meas. Sci. Technol. **32** (2021) 074004 (10pp)
https://doi.org/10.1088/1361-6501/abe81c

Interferometric device for the in-process measurement of diameter variation in the manufacture of ultraprecise spheres

Rudolf Meeß[1,*], **Dennis Dontsov**[2] and **Enrico Langlotz**[2]

[1] Physikalisch-Technische Bundesanstalt, Braunschweig, Germany
[2] SIOS Meßtechnik GmbH, Ilmenau, Germany

E-mail: rudolf.meess@ptb.de

Received 16 December 2020, revised 1 February 2021
Accepted for publication 19 February 2021
Published 5 May 2021

Abstract

A novel device is presented which is designed for in-process measurements of the variation of the diameter of highly reflective spheres. Silicon spheres have been used for the new definition of the International System of Units (SI). Many spheres have to be processed, and the form of these objects, and thus the manufacturing process's stability, needs to be controlled every day. Commercially available measurement equipment and even state-of-the-art spherical interferometers have reached their limits in terms of resolution, uncertainty, the complexity of their handling routines, measurement time and even financial investment. A novel setup has thus been designed after considering and selecting a special mechanical setup with a minimal measurement loop, stable optical sensors and a handling strategy which avoids collision and contact with the very valuable, superpolished spherical objects. Thus, the design minimizes the influence of the environment and reduces the measurement time at an equator with sub-nanometre resolution to 3 min. In addition, the analysis time is reduced to less than a minute.

Keywords: in-line measurement, sphere, non-contact measuring system, dimensional metrology for process optimization

1. Introduction

Scientific discussions about a more precise determination of the Avogadro constant using silicon spheres and related experiments started in the early 1970s [1]. The spheres are made of very pure material, and they must comply with very challenging geometric specifications to achieve an overall relative measurement uncertainty of 10^{-8} in this project. All spheres made of the enriched ^{28}Si isotope that are used for the Avogadro Project are either manufactured at the Physikalisch–Technische Bundesanstalt (PTB) or reworked and finished at PTB. The international Avogadro Project ended with World Metrology Day on May 20, 2019, when the definition of the kilogram changed from being based on an artefact to being defined through fundamental constants. An overview and the scientific classification of this project can be found in [2–5].

1.1. Manufacturing chain for silicon spheres

There are several technical specifications for the spheres, which need to be fulfilled by the manufacturing process. The mass has to be 1 kg with a tolerance of about 100 mg. The deviation in form must be less than 100 nm. The surface integrity must be ensured, with a average roughness of less than 1 nm. Finally, there must not be metallic contamination on the surface.

* Author to whom any correspondence should be addressed.

Figure 1. Process steps in the manufacture of silicon spheres.

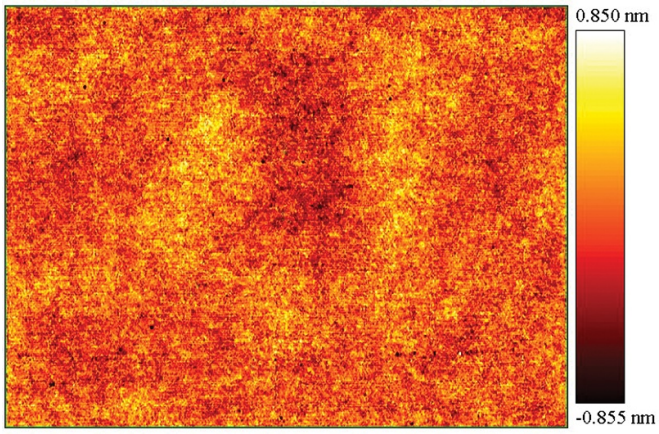

Figure 2. Typical topography of a finished silicon sphere. The measured area is 416 µm × 312 µm, Sa = 0.224 nm (phase shifting interferometry, ×20 Mireau lens, quartic correction).

A novel manufacturing chain for silicon spheres was therefore developed at the PTB [6]. The final polishing process is based on a physical removal mechanism, as opposed to the classical manually operated methods of an optician.

Figure 1 depicts the steps of the manufacturing chain. From left to right, the cut ingot and the early state of a cut sphere are shown, followed by a turned and then a lapped sphere with its typical 'semigloss' surface appearance. On the right, a superpolished sphere can be seen. Figure 2 shows a scan of the typical topography of the finished surface.

For the polishing process, a non-contact measurement of three equators with an accuracy in the nanometre range is sufficient for process control. Due to the high cost of an ingot and the long processing time, daily control of the form is chosen for quality control of the polishing process as well as measurement of the mass and optical inspections.

Unfortunately, neither PTB's form-measurement devices nor their sphere interferometers can be used non-stop for daily measurements, since both types of device are used for other tasks, sometimes even tasks mandated by legislation. Furthermore, due to the use of pitch-based processes for manufacturing, the downtime for measurements must not be longer than one day.

1.2. Form measurement

The measurement principle of the PTB's sphere interferometers is based on interferometry with spherical reference faces

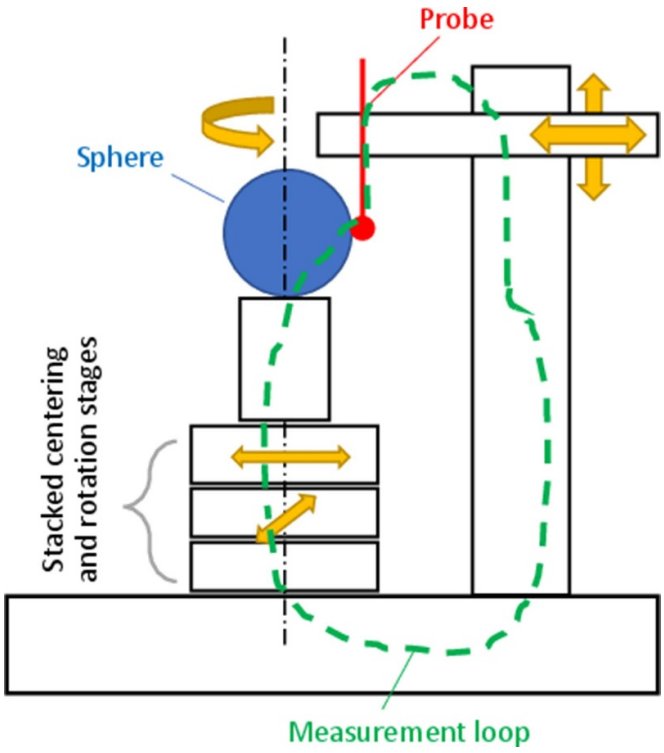

Figure 3. Typical setup of a conventional form measurement device. The measurement loop (green dashed line) contains both the sphere and all the positioning, centring and rotating devices.

[7]. Their design and measurement results are reported in [8–13]. Another setup with flat reference plates is used at the National Metrology Institute of Japan, see [14]. Furthermore, a setup with a flat reference plane and combined phase-shifting and frequency-sweeping interferometries is reported in [15].

What all these approaches have in common is that determination of the spherical volume is time-consuming, the measurement devices are not commercially available, and they need skilled operators.

Commercially available form measurement devices for line scans usually have a stacked mechanical setup, see figure 3. A probe, a rotating axis and a complete positioning system are part of the measurement loop, and their mechanical and thermal stability are crucial for the measurement uncertainty.

Exceptionally precise mechanical components are needed for a measurement device with single nanometre resolution and repeatability that uses a finite number of revolutions and measurements. However, a crucial task for devices with this kind of measurement loop is the separation of spindle error from artefact form error. Several approaches are well known and established [16–19]. Basically, multiprobe approaches [20], different sensor positions [21] or numerous measurements lead to a decrease in uncertainty for the numerical results of the form error. Ideally, no artefact needs to be involved [16].

2. Design and realization

Due to the high symmetry of the spheres, the measurand of the device is the diametric variation of the equator. The curvature

of the artefacts is approx. 50 mm. The surface is polished with roughness values in the range from an average roughness Sa = 1 nm down to Sa = 0.1 nm; see figure 2. The objects are made of single-crystal silicon: the cubic crystal leads to symmetric form errors of the sphere in the shape of a tetrakis hexahedron or rhombic dodecahedron, both Catalan solids. The relevant characteristics for the manufacturing and measurement of anisotropic materials are described in [22–24].

The measurement must be made in non-contact mode. The safe handling of these valuable objects must be assured by collision-free kinematics; there must be no risk of scratches or slipping motions of the spheres. The measurement requires single nanometre resolution and repeatability. The diameter variation is in the range from a single nanometre up to 200 nm, with a slope up to 20 nm/45° on the spherical surface. Short measurement times $t_m < 1$ h are desirable, with a short numerical processing delay $t_p < 5$ min before getting the numerical results. The environment is an air-conditioned ultra-precision workshop with an air shower and a constancy of temperature of approx. 0.5 K, 20% rh–90% rh.

As a desirable feature, the device should be easy to use with an easy and fast adjustment procedure and operation. It should require low investment and it should be maintenance-free. Finally, there must be no danger to the operator from the device. This includes electrical, mechanical, and optical aspects.

2.1. Concept

The concept for form measurement at the nanometre level includes a adequate thermal concept, a suitable probe system, and a suitable concept for moving the object of interest.

Neither areal nor absolute data are necessary for daily in-process measurements due to the high grade of symmetry and low-to-mid spatial frequencies of the processed spherical surfaces. Hence, line scans of at least three arbitrary, but perpendicular equators have been found to be sufficient for this purpose. Diametric variation is a sufficient measurand for the assessment of the form error of the known kinds of geometrical errors of the silicon spheres.

By determining the sum of two signals [20], the accuracy of the positioning system can be taken out of the calculation of the measurand. This does not affect the result if the boundaries are chosen properly. No compensation for any error in the motion of the positioning devices is necessary.

A sketch of the proposed system with its compact and stable design is shown in figure 4.

2.2. Probe

Capacitive sensors with sub-nm resolution have been tested, but they were not able to detect the semiconductor's surface properly due to charging. Furthermore, the distance in the micrometre range between the sensor and the sphere is too small for safe handling and thus operation. Interferometry was chosen, as it is a known technology for collimated or focused distance measurement [25]. A commercially available He-Ne laser with a wavelength of 632.8 nm was chosen. The stability

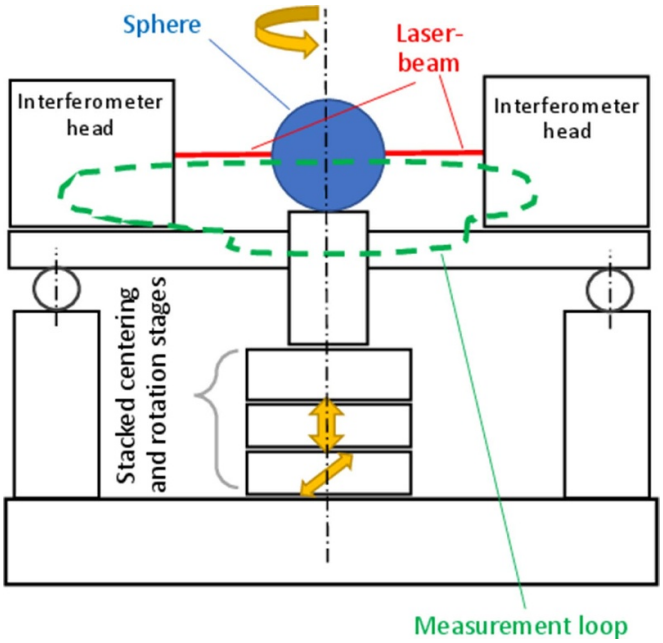

Figure 4. Setup of proposed device with a significantly reduced measurement loop (green dashed line).

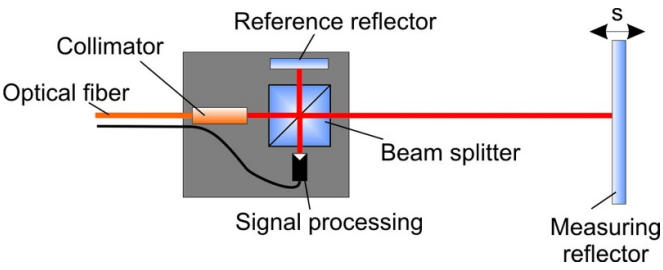

Figure 5. Sketch of the interferometer head.

of the frequency after warming up is 2×10^{-8}, the spot size of the connected measurement beam is approx. 30 µm, and the resolution of the signal is less than one nanometre. The interferometers are of the single beam homodyne type. The devices use the single frequency of a stabilised HeNe laser to determine the displacement.

The design corresponds to the Michelson principle. The plane waves from a laser light source are split into two coherent partial waves, which are then superimposed and interfere. The interferometers are also designed according to the plane mirror principle. Only a single beam is emitted by the interferometer, which is then reflected into itself by the measuring surface; see figure 5. The advantage of this setup is that it has a single measuring point, which is small and very precisely defined. The surface of the target can be used for probing without an additional reflector, whereby minimum reflectance levels of up to about 1% are possible [26].

The laser source as well as the supply and evaluation unit of the interferometers are spatially separated from the measuring head by means of a fibre coupling. The heat sources are efficiently separated from the measuring head and do not affect

the measurement results, e.g. the power supplies and amplifiers. Moreover, additional optical elements for beam guidance can be easily integrated and their adjustment takes place outside the enclosure.

The main factors influencing the interferometric length measurement are the refractive index of air and the vacuum wavelength of the laser used, or its stability [26]. The refractive index of air is a function of temperature, pressure, humidity, and further minor influencing variables. If the influencing variables are measured, a mathematical correction is implemented, using the Edlén formula [27].

Due to the interpolation methods used during signal demodulation, the resolution is better than 0.1 nm with nonlinearities below 2 nm.

To ensure the lowest possible inherent thermal drift behaviour, the interferometers are specially adapted. A steel alloy is chosen with a coefficient of thermal expansion close to that of glass. Thus, the influence of temperature changes on the structure is low and results in minimal additional internal stresses of the assembled and carefully adjusted components due to homogeneous expansion of the different materials.

Furthermore, stainless steel has low heat conductivity. Dimensional changes in the structure take place over a long timescale, compared to short-term disturbances, namely the placing or even the replacing of the spheres and the opening of the enclosure within several seconds.

A further modification of the interferometer head is a tiltable plane-parallel glass plate, which is integrated into the measuring arm. Therefore, the measurement axes of the interferometers can easily be shifted laterally by tilting the plates. Finally, the interference signal evaluation needs to be adapted to allow direct probing of the polished spherical surface.

No additional components such as triple or planar mirrors are needed to couple the object and the interferometric device. The collimated beam does not require a focusing lens. With the given curvature of the spheres, a signal strength of 65% can be achieved.

Moreover, the dead path is reduced to a meaningful minimum. Two interferometers are used. A design with a single interferometer head with a split reference path and a second beam on the opposite side of the sphere would enlarge the free beam path, make it significantly more sensitive to mechanical misalignment and thermal influences, and would also increase the effort involved in the adjustment of the beam path. Two heads of a proven industrial standard are thus chosen for the design of the measurement loop.

2.3. Positioning concept and measurement loop

There are three main characteristics of the positioning and the metrology loop. First, the measurement loop is completely decoupled, see figure 4. This is only meaningful and possible due to the known wavelengths and amplitudes of the form errors of the spheres. Since the eccentricity of the positioning system is much lower than the typical wavelength of the form error, the influence on the measurement result is very low. This will be discussed in detail later. Furthermore, the stacking of the axis does not affect the measurement loop because it is not coupled to it or part of it and thus it does not affect the sum of the distance signals. Third, the metrology plate and the base of the positioning devices are linked with a kinematic coupling. This kind of coupling is completely free of outside forces on the metrology plate and leads to excellent structural stability of the metrology loop.

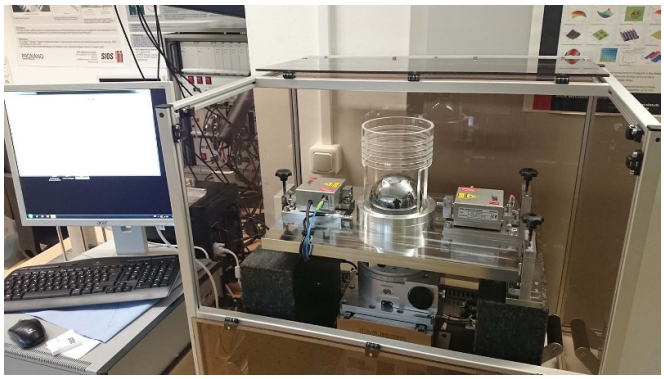

Figure 6. Photo of device with opened thermal enclosure.

2.4. Thermal concept

The sensor heads, the baseplate for the sensor heads and all components of the measurement loop are made of the same stainless steel to avoid internal stresses due to different coefficients of thermal expansion.

In addition, the complete setup is enclosed in a transparent polycarbonate housing to avoid any convective influences from the environment even though the equipment is kept stable to within 0.5 K without any daylight or alternative heat sources.

2.5. Setup

The first setup was built at PTB and tested under laboratory conditions [28]. The proof of concept led to a collaboration with the SIOS company to place the responsibility for the system into a single administration. Thus, the mechanical setup, interferometry and the driving software have been designed as a complete system. The system is shown in figure 6.

Since handling is a crucial part of the manufacturing and measuring procedures of the valuable and sensitive spheres, the transport and integration of the spheres into the measurement device needs special attention.

A cylinder of polymethyl methacrylate (PMMA) with a base of polyetheretherketone is used to support the spheres. This container can be seen in the centre of the setup in figure 6. The use of this cylinder as a transport cage means that the lowest point of the sphere is above the lowest edge of the support. When the cylinder is put on a table, the sphere does not touch it. As soon as the cylinder has been positioned in the measuring device, the original support is replaced by the machine's concentric support, and the cylinder then acts as a windshield.

The sphere is placed into the cylinder with an additional columnar support. The PMMA cylinder thus enables the contactless transport of the sphere before and after the measuring

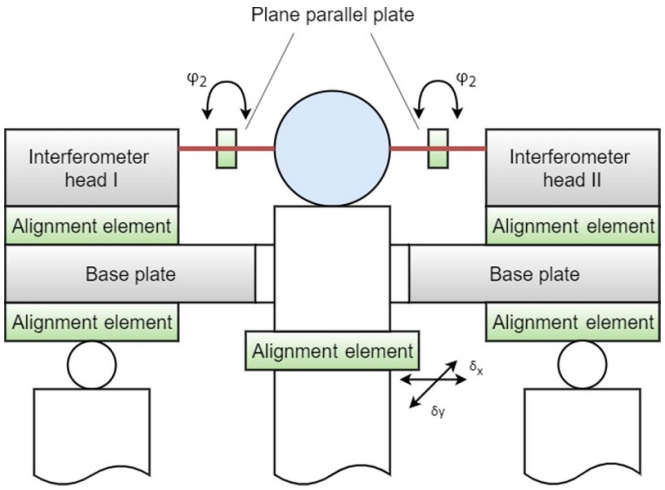

Figure 7. Adjustment of interferometer heads.

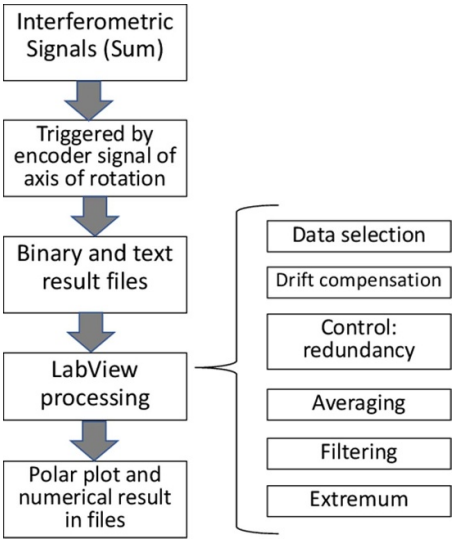

Figure 8. Information flowchart and processing scheme.

procedure, and it acts as an additional thermal shield and as a windscreen in the interferometric device during the tempering phase and the subsequent measurement.

2.6. Alignment of the measurement loop

The elements involved in the alignment are shown in figure 7. The parallelism of the two measurement axes of the interferometers is adjusted using a prismatic optical alignment assembly and a test telescope. The orientations of the interferometer beams are aligned by means of two pivots for each interferometer head. The heads are tilted in two perpendicular planes perpendicular to the beam. The positions of these alignment elements underneath the heads can be seen in figure 7. The beam parallelism is better than 50 µrad.

The coaxiality of the beams is then adjusted using the interferometers' signal processing units. The integrated plane-parallel glass plates enable a parallel offset of the measurement beams.

The beams are shifted by tilting the plane-parallel plates (ϕ_2 in figure 7) until the opposite beam enters the interferometer and produces a sufficient measurement signal. With this method, the coaxiality is better than 100 µm.

The adjustment of the perpendicularity of the coaxial measuring beams of the interferometers and the axis of rotation of the sphere is realized by three vertically adjustable kinematic couplings of the baseplate, symbolized by the alignment elements underneath the base in figure 7. The baseplate can be tilted over two perpendicular axes. A sphere with high waviness is inserted into the measurement setup for this purpose. Significant mid-spatial frequencies on the millimetre scale are necessary. The redundancy of the results is an indicator of the perpendicularity. Each turn must exhibit two identical halves of the sum-signal because both interferometers must detect the same points on the sphere. Otherwise, the equator of rotation is different from the scanned equators.

The eccentricity of the sphere's support is minimised by rotating the test sphere and evaluating the distance values of both interferometers with the help of the integrated alignment slides for centring. The sphere's support can be moved by amounts δ_x and δ_y relative to the axis of rotation of the rotary table; see figure 7.

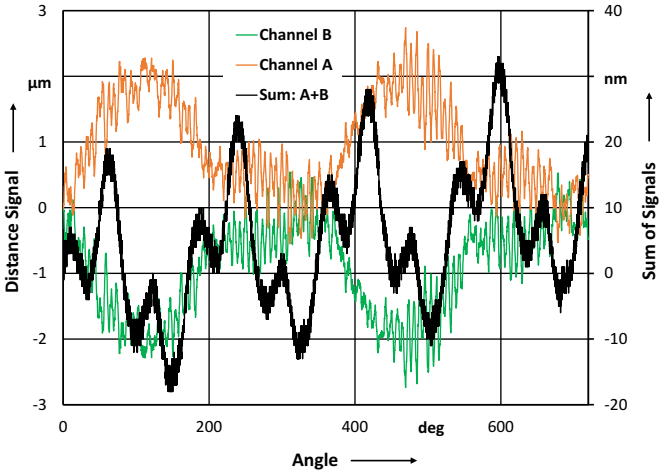

Figure 9. Typical measurement data: two revolutions, with collinear interferometric distance signals A and B and the sum of both signals A and B as the measurand diameter variation.

2.7. Signal processing

Signal processing and the flow of information are shown in figure 8. The control of the measurement unit is driven by C++ routines, while the processing results are programmed in LabView.

Figure 9 shows a typical measurement result for a silicon sphere. The green and orange lines are the direct distance signals of both interferometers. Due to the short free beam paths of the opposite arrangement, environmental influences are minimized while summing both signals.

The sum of interferometer signals A and B is the variation of the diameter of the sphere along an equator. Due to the synchronicity of the captured distance signals A and B, the sum is

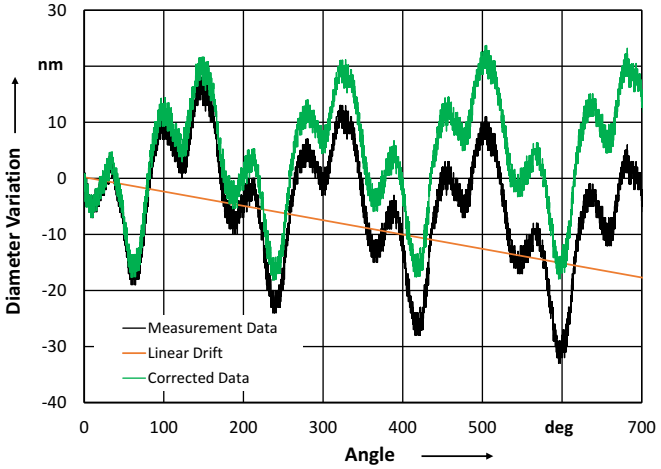

Figure 10. Typical diameter variation measurement signal (black line) and drift-compensated signal (green line), assumed drift shown as a red line, arbitrary origin.

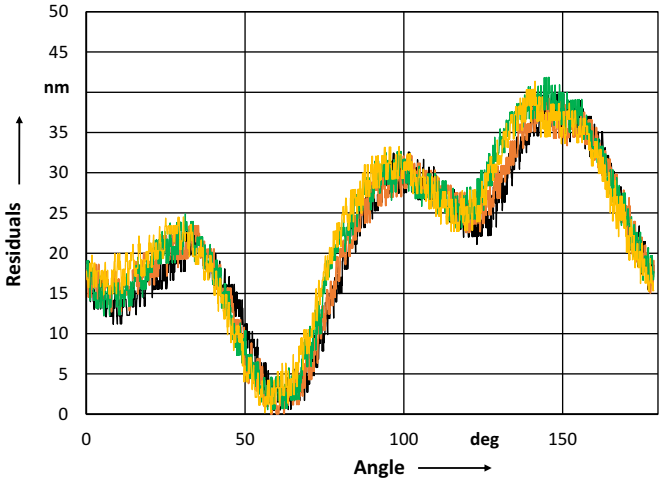

Figure 11. Overlay of the four captured half equators of a two-turn measurement; control for redundancy and noise.

the exact value at each trigger position. Hence, the result has nanometre precision while the source signals have perturbations in the range of micrometres. Due to the design of the device and the sign of the signals, the mechanical perturbation due to a shift of the sphere is non-destructive for the sum of both signals.

The subsequent step in data processing is the automatic or manual correction of drift. A typical result is shown in figure 10. After tempering for several minutes, the typical thermal drift is in the range from 10 nm to 50 nm.

By dividing the captured data from 720° of rotation into four redundant parts, these overlaid measurements yield a good control for noise and redundancy; see figure 11. The signals in figure 11. are unfiltered.

In the next step, the average of all four measurements is processed and filtered by means of a simple low band filter with a lower cut-off frequency of 0.015. Typical residuals of

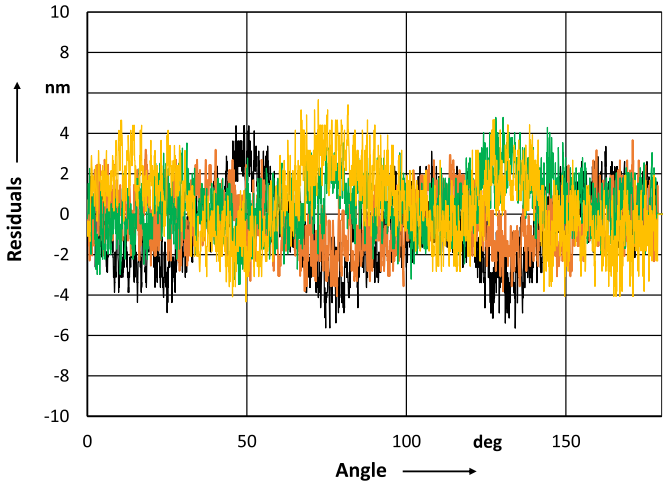

Figure 12. Residuals of the two-turn measurement.

the four parts are shown in figure 12. They are in the range of single nanometres.

Finally, the results are visualized in the polar plot of a record; see figure 13. The numerical value of the span of the diametric variation is given in the plot. Thus, all the important geometrical and numerical information is shown. The span of the diametric variation of the data processed, as before, is 35.56 nm in figure 13.

3. Sources of error and measurement uncertainty

Temperature, pressure, relative humidity and the concentration of carbon dioxide all influence the refractive index of air. A 1 °C change in temperature, a 2.5 mm Hg change in air pressure, or an 80% change in relative humidity will cause a 1 ppm error. Temperature and absolute air pressure sensors are placed near the free laser beams. The correction, in accordance with the Edlén equation [27], is done in-process.

The length of the laser beams of both arms in air is approx. 10 mm and the measurement time is 6 min. The stability of the frequency of the laser source is better than 10^{-8}. The influences on the change of the sum of two very close and almost identical short beams and signals at the single nanometre level are minimal and are neglected here.

3.1. Surface layers

The surface layers of a sphere affect the distance measurements. The first sublayer in the silicon bulk is an intermediate layer of silicon oxide (SiO), which is followed by a layer of SiO_2. This layer is covered by a layer of chemisorbed water. Finally, a carbonaceous contamination layer is observed, for more details see [29]. The overall thickness of these layers is measured to be in the range of 2 nm to 6 nm on the spheres AVO28-S5 and AVO28-S8. The variation of the layers does

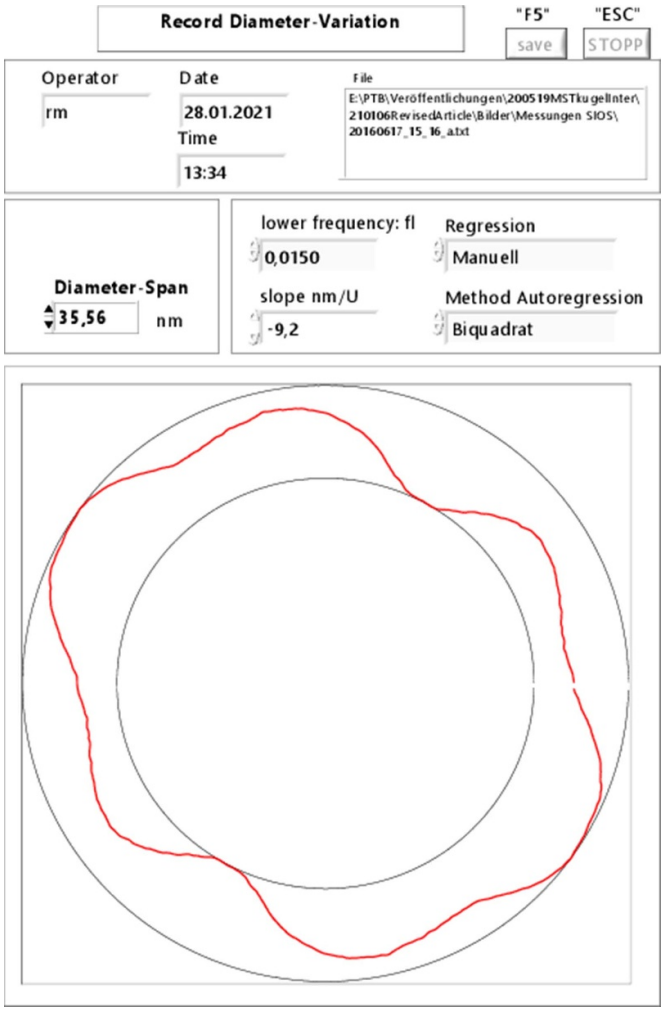

Figure 13. Typical record of data processing with polar plot; diameter span is 35.56 nm. Point symmetry is significant.

not exhibit a large degree of symmetry here and the layers are very thick, which may be due to the special finishing process of the spheres in this study.

Later measurements revealed a higher degree of uniformity of the layers for differently finished surfaces [7]. The complete surface layer has a thickness of less than 2 nm. This is the result of the finishing process at PTB. This distribution was detected on all other spheres investigated.

The sum of the two opposite signals of the measurement device proposed here is affected by the refractive indices of the surface layers. In the non-realistic and most adverse case of an assumed pure reflective layer, lying opposite an optically inactive layer on the sphere, an error of 4 nm in diameter variation can be expected. In practice, the influence of the dominant optically active oxide layer with its thickness of approximately 1 nm can be neglected, particularly because of its uniform and symmetric distribution; see [7].

Finally, no absolute diametric values are determined here, rather changes in the sum of signals. Additional layers with constant thicknesses and properties do not affect the measurement results within a meaningful range.

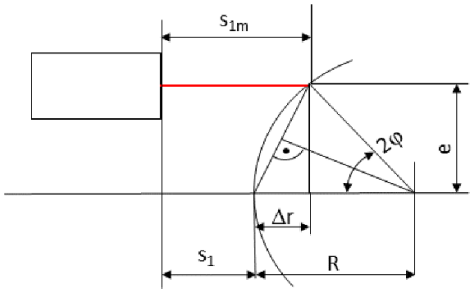

Figure 14. Sketch of a sphere with radius R.

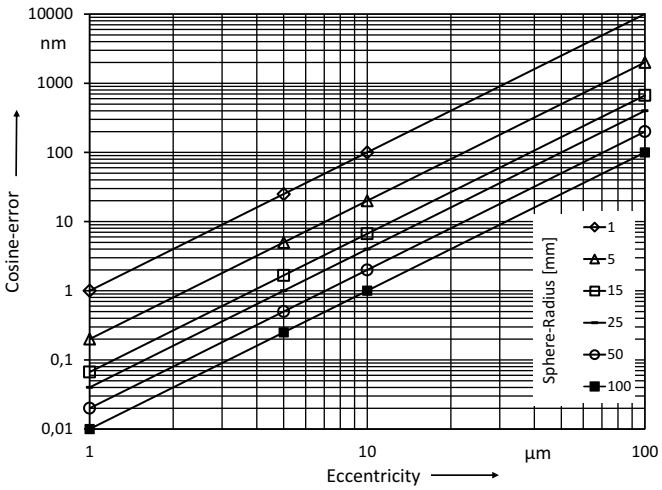

Figure 15. Cosine error $2\Delta r$ due to eccentricity of the sphere.

3.2. *Kinematic errors*

A sketch of a typical misalignment due to the eccentricity of a spherical artefact is shown in figure 14.

The measurand of the optical sensor system with a rotating spindle is s_{1m}. Here, the eccentricity e of the artefact is due to a misalignment of the sphere's centre and the measurement beam's axis, shown by the red line in figure 13. The error in the distance measurement Δr is then

$$\Delta r = s_{1m} - s_1 = R(1 - \cos 2\varphi),$$

with

$$\sin 2\varphi = \frac{e}{R}$$

and

$$\tan \varphi = \frac{\Delta r}{e}.$$

It can be seen in figure 15 that for a spherical radius of 50 mm, an eccentricity of 5 µm leads to a cosine error of $2\Delta r < 1$ nm in diameter.

This is a value for the mechanical centring of a sphere that can be reached with conventional precision machining technologies, combined with properly adjusted and centred sphere supports.

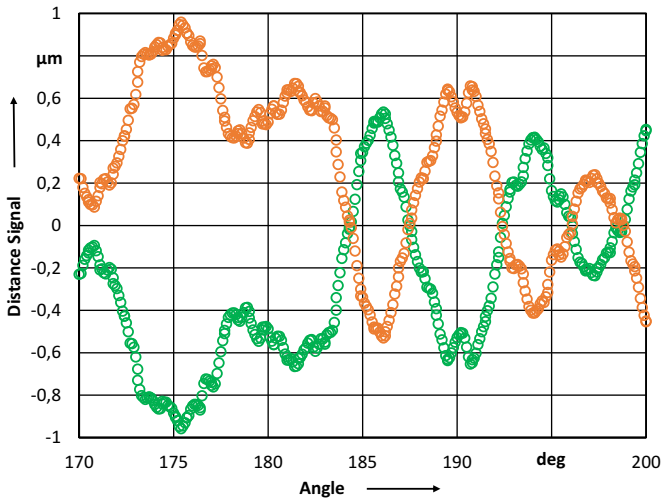

Figure 16. Slope and resolution of the recorded primary data points of both channels.

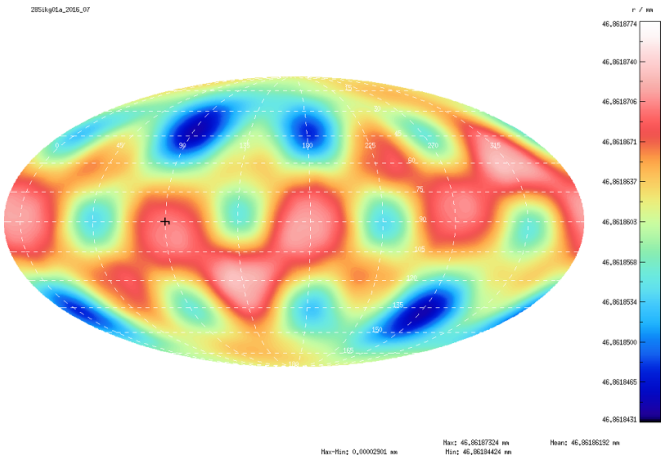

Figure 17. Mollweide plot of the topography of sphere 'Si28kg01a' as measured by PTB's sphere interferometer. The form deviation is 29 nm and is represented by a colour range from blue to red.

A second source of kinematic error is the misalignment of the collinear measuring beams. Rotating the sphere, ideally by 180°, means that a measured point is not in the measurement path of the second interferometer. This leads to non-redundant results. Thus, the beams are aligned with an autocollimator of better than 100 µrad. A prism is integrated into the beam path at the centre of the rotational axis for this adjustment. Taking the typical wavelength of several millimetres of form errors of the spheres into account, a lateral shift of less than 1 µm cannot affect the distance measurements.

3.3. Synchronicity of data acquisition

A typical run of measurements is shown in figure 9; a close-up of this run is given in figure 16. The primary measurement data show mid-frequency radial error motions of the rotational axis. The data acquisition of both interferometer signals must be fast and sufficiently synchronous, and the slope of the radial deviations must be resolved sufficiently. This is achieved by triggering the data acquisition of both interferometer signals using the encoder signal of the rotational axis at a microsecond level. In figure 16, it can be seen that a complete steep rise is resolved with at least five synchronized data points.

A detailed determination of the uncertainty in the measurement will be part of the work undertaken in the future.

4. Results

The results of the PTB sphere interferometer are used here to assess the quality and reproducibility of the system that was developed. As an example, a Mollweide plot of the silicon sphere 'Si28kg01a' is shown in figure 17. The form error is determined to have a value of 29 nm peak-to-valley.

Figures 18 and 19 show the results of the measurement of two equators by the proposed system. The given values are

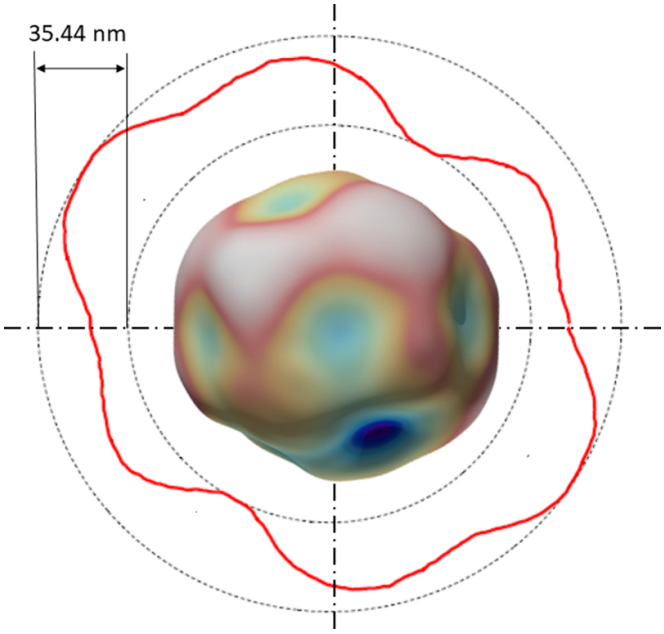

Figure 18. Polar plot of the results for sphere 'Si28kg01a' with a diametric span of 35.44 nm. In the centre: corresponding projection of the error model of measurement obtained by PTB's sphere interferometer.

diametric spans, so they must have twice the value of the form error, with implied perfect symmetry.

At the centre of the plots in figures 18 and 19, the corresponding 3D projections of the measurements of the sphere interferometer are overlaid to gain an impression of how consistent both measurement concepts and systems are.

With the experience of hundreds of measurements of equators and the opportunity to compare these with the results of the spherical interferometer, it can be concluded that a total of at least five measured equators, half of the determined diameter span, come close to the value of the form error as determined by PTB's sphere interferometer.

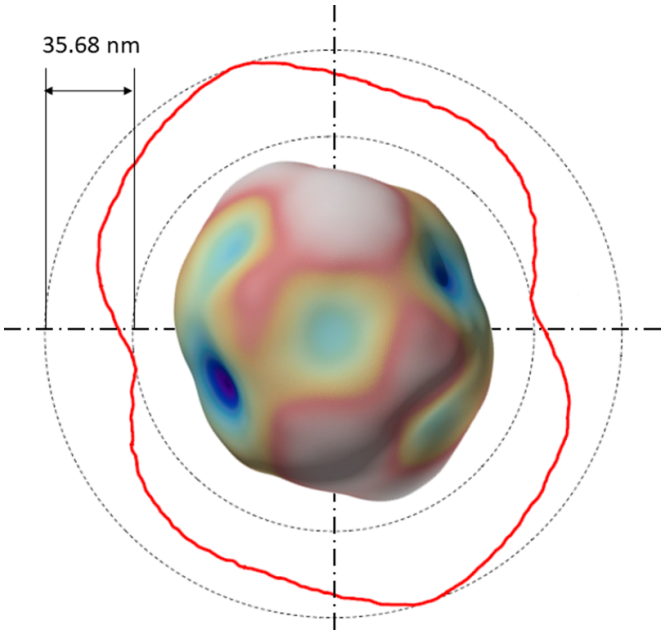

Figure 19. Polar plot of the results for sphere 'Si28kg01a' with a diametric span of 35.68 nm. In the centre: corresponding projection of the error model of measurement obtained PTB's sphere interferometer.

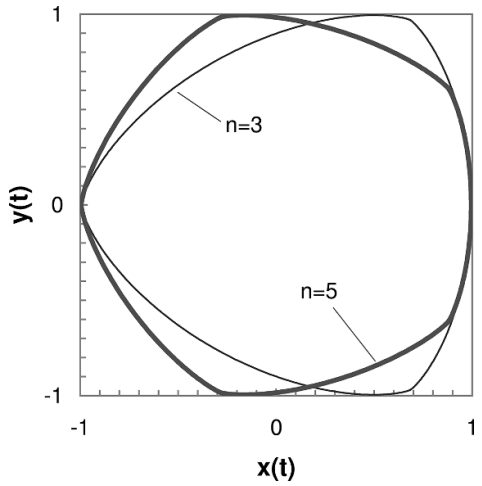

Figure 20. Orbiform curve with $n = 3$ and $n = 5$ sides.

5. Discussion

A measurement device for diameters that uses two opposite measurement points on a sphere is not capable of detecting odd-numbered polygons such as the orbiforms shown in figure 20. The orbiform is a typical form error when manufacturing spheres with conventional planar or grooved tools in a rolling manner. Due to the high degree of symmetry and the preferably even-numbered polygons on the equator in the polishing process used here, this effect has a lower influence on the numerical results of the silicon spheres. An orbiform has been detected by the sphere interferometer on only a few incorrectly processed spheres.

The highly reflective surface of a silicon sphere with an almost perfect spherical shape allows its use as a mirror for the laser beam. The setup was also tested with a focusing lens in front of the interferometer head. Focusing on the surface allows the measurement of transparent objects.

However, this optical setup results in further degrees of freedom for the alignment. As well as the adjustment of opposite positions of the measurement spots on both sides of the sphere, even the distances of the sensor heads to the sphere must be adjusted. Thus, collimated beams are chosen for the final setup with the requirement for a predominantly reflective surface.

The distance between the sensor head and sphere was chosen to be as short as possible to keep the beam length in air as short as possible and thus reduce the environmental influence. The interferometers can measure centimetres of shift at larger distances from the moving objects with the same resolution, but are then much more sensitive to changes in the density and flow of the environmental air.

In the first setup, the interferometer heads are solely adjusted by means of two pivots of the interferometer heads; see figure 7. Coaxiality and parallelism must then be adjusted as an iterative process. Tiltable plane-parallel glass plates in the measuring arms of each of the two interferometric sensors allow a sequential procedure and this reduces the adjustment time drastically.

Evaluating the overall measurement performance of the system, it needs to be emphasized that the adverse thermal drift of a sphere during the measurement, as shown in figure 10, is almost as large as the measurement result of figure 13.

In spite of the simple linear model for the thermal drift of the sphere, the measurement results reveal repeatability and redundancy at the single nanometre level. The thermal stability of the complete setup allows the separation of the thermally induced dimensional changes of the sphere. No thermally or mechanically induced stresses influence the rest of the metrology loop. This highly repeatable and accurate characteristic of the complete instrument, including the object to be measured, is the result of the specific design. The adapted probe and the thermally and mechanically stable structure collaborate best with the almost perfectly smooth silicon surface with a curvature of approx. 100 mm, its bulk mass of 1 kg, and its very homogenous thermally induced change of volume inside the instrument.

The purpose-built device is realized with two commercially available laser interferometers with design adjustments on the part of the manufacturer. The thermal characteristics of the heads are optimized by equalizing the components' thermally induced dimensional changes. The internal signal processing of the heads is adjusted to the spherical reflector and the beam is made to be adjustable for a meaningful alignment procedure.

The principal suitability of the device as proposed is shown in the experience gained while continuously measuring numerous spheres for several months. The quality of the numerical results and the similarity to the results of PTB's sphere interferometers are given.

6. Conclusions

A novel device for the in-process determination of the variation of the diameter of super-polished silicon spheres is introduced. The interferometric setup is very compact and thermally stable. It exhibits sub-nanometre resolution with single nanometre noise and repeatability. Measurement times of 6 min are realized for a single equator, and the numerical processing of the results is completed within a few minutes. Furthermore, the new equipment does not require calibration routines for the compensation of kinematic errors of the rotating spindle or the guiding elements.

The device is suitable for daily use, easy to use and gives fast results. The spheres can be handled safely without danger of mechanical damage due to the special transport and insertion subassembly.

In a next step, the device will be capable of performing form measurements by integrating an ultra-precise spindle with a single-nanometre asynchronous error motion.

ORCID iDs

Rudolf Meeß https://orcid.org/0000-0002-9009-8034
Dennis Dontsov https://orcid.org/0000-0002-5171-9264
Enrico Langlotz https://orcid.org/0000-0002-5425-1070

References

[1] Deslattes R D, Henins A, Bowman H A, Schoonover R M, Carroll C L, Barnes I L, Machlan L A, Moore L J and Shields W R 1974 Determination of the Avogadro constant *Phys. Rev. Lett.* **33** 463
[2] Becker P 2001 *Rep. Prog. Phys.* **64** 1945
[3] Becker P, Friedrich H, Fujii K, Giardini W, Mana G, Picard A, Pohl H-J, Riemann H and Valkiers S 2009 *Meas. Sci. Technol.* **20** 092002
[4] Becker P, Bettin H, Danzebrink H-U, Gläser M, Kuetgens U, Nicolaus A, Schiel D, De Bièvre P, Valkiers S and Taylor P 2003 *Metrologia* **40** 271
[5] Nicolaus R A, Bartl G, Bettin H and Borys M 2013 *IEEE Trans. Instrum. Meas.* **62** 1499–505
[6] Meeß R, Hinzmann G and Lück A 2015 *Proc. 15th EUSPEN Int. Conf.* p 355
[7] Bartl G *et al* 2017 *Metrologia* **54** 693
[8] Nicolaus A and Bönsch G 1997 *IEEE Trans. Instrum. Meas.* **46** 563
[9] Nicolaus A and Bartl G 2018 Fizeau interferometry for the sub-nm accurate realisation of sphere radii *Modern Interferometry for Length Metrology: Exploring Limits and Novel Techniques* vol 1 (Bristol: IOP Publishing) pp 3-1–13
[10] Bartl G, Krystek M, Mai T, Nicolaus A, Peter A and Spolaczyk R 2014 *Classical Optics 2014, OSA Technical Digest OTh3B.3*
[11] Mai T and Nicolaus A 2017 *Metrologia* **54** 487–93
[12] Azuma Y *et al* 2015 *Metrologia* **52** 360–75
[13] Bartl G, Bettin H, Krystek M, Mai T, Nicolaus A and Peter A 2011 *Metrologia* **48** 96
[14] Kuramoto N, Fujii K and Yamazawa K 2011 *Metrologia* **48** S83
[15] Wu X, Li Y, Wei H, Yang H, Yang G and Zhang J 2013 *Meas. Sci. Technol.* **24** 115202
[16] Evans C, Hocken R and Estler W T 1996 *CIRP Ann.* **45** 617–34
[17] Whitehouse D J 1976 *J. Phys. E: Sci. Instrum.* **9** 531–6
[18] Grejda R, Marsh E and Vallance R 2005 *Precis. Eng.* **29** 113–23
[19] Marsh R 2008 *Precision Spindle Metrology* (Lancester, PA: DEStech Publications)
[20] Moore D 1989 *J. Phys. E: Sci. Instrum.* **22** 339
[21] Marsh E, Couey J and Vallance R 2006 *ASME J. Manuf. Sci. Eng.* **128** 180–7
[22] Masolin A, Bouchard P, Martini R and Bernacki M 2013 *J. Mater. Sci.* **48** 979–88
[23] Sato K 1998 *Sensors Actuators* A **64** 87–93
[24] O'Connor B P, Marsh E R and Couey J A 2005 *Precis. Eng.* **29** 124–32
[25] Castro H F F 2008 *Measurement* **41** 526–37
[26] Schott W, Dontsov D and Pöschel W 2009 *Tech. Mess.* **76** 239
[27] Birch K P and Downs M J 1994 *Metrologia* **31** 315–6
[28] Meeß R, Drösemeyer H, Langlotz E, Schott W and Dontsov D 2018 *Proc. 18th EUSPEN Int. Conf.* p 133
[29] Busch I, Azuma Y, Bettin H, Cibik L, Fuchs P, Fujii K, Krumrey M, Kuetgens U, Kuramoto N and Mizushima S 2011 *Metrologia* **48** S62